Decadal and Interannual SST Variability in the Tropical Atlantic Ocean

JAMES A. CARTON,* XIANHE CAO,* BENJAMIN S. GIESE,+ AND ARLINDO M. DA SILVA@

*Department of Meteorology, University of Maryland, College Park, Maryland
+Department of Oceanography, Texas A&M University, College Station, Texas
@Laboratory for Atmospheres, NASA/Goddard Space Flight Center, Greenbelt, Maryland

(Manuscript received 3 January 1995, in final form 9 September 1995)

ABSTRACT

The mechanisms regulating interannual and decadal variations of sea surface temperature (SST) in the tropical Atlantic are examined. Observed variations of sea surface temperature are typically in the range of 0.3°–0.5°C and are linked to fluctuations in rainfall on both the African and South American continents. The authors use a numerical model to simulate the observed time series of sea surface temperature for the period 1960–1989. Based on the results, experiments are conducted to determine the relative importance of heat flux and momentum forcing. Two dominant timescales for variability of SST are identified: a decadal timescale that is controlled by latent heat flux anomalies and is primarily responsible for SST anomalies off the equator and an equatorial mode with a timescale of 2–5 years that is dominated by dynamical processes. The interhemispheric gradient of anomalous SST (the SST dipole) is primarily linked to the former process and thus results from the gradual strengthening and weakening of the trade wind system of the two hemispheres.

1. Introduction

Sea surface temperature (SST) is an important component of the coupled ocean–atmosphere system. In the Tropics warm SST is associated with enhanced convection and shifts in trade wind strength and direction. Cool SST is associated with subsidence, shallow and strongly stratified atmospheric boundary layers, and low-level clouds. A striking example of the importance of interannual fluctuations of SST for the tropical Atlantic climate is provided by historical rainfall time series in the northern Nordeste region of Brazil (Fig. 1a). During the mid-1970s and mid-1980s rainfall was unusually heavy, whereas during the early 1980s, this region experienced persistent drought. A corresponding, highly correlated, time series of interhemispheric SST differences is shown in Fig. 1b (histogram). The influence of these low-frequency SST anomalies on rainfall distribution occurs through their effect on surface air pressure (Hastenrath and Greischar 1993a,b). A northward gradient of anomalous SST induces a southward gradient of anomalous pressure causing the intertropical convergence zone to shift northward. The northern Nordeste region of Brazil lies at the southern edge of the normal range of the ITCZ. Under these anomalous SST conditions the ITCZ never descends to the northern Nordeste and drought occurs. Thus, tropical rainfall patterns appear particularly sensitive to the interhemispheric gradient of SST anomaly, rather than the anomalies themselves. Anomalous SSTs have also been related to rainfall variations over the African subcontinent (Folland et al. 1986; Lamb and Peppler 1991) and rates of hurricane formation (Gray and Sheaffer 1991).

Near the equator the strongest variations of SST occur in the eastern ocean. The variability there results from both warm and cool events. During the three decades beginning in 1960, nine events occurred when the warming exceeded 0.5°C; the most dramatic warming occurred in 1963. These warm events have important local climate effects. In particular, they are associated with flooding in the coastal cities of the Gold and Ivory coasts (Hisard 1980; Wagner and da Silva 1994; Carton and Huang 1994). During the same period five anomalous cold events occurred.

The warm events occur primarily in Northern Hemisphere summer, when equatorial upwelling normally cools the surface water. In spring following a winter when the off-equatorial trade winds weakened substantially or in a spring during which the equatorial trade winds weaken substantially, a relaxation occurs in the equatorial thermocline shifting heat eastward. The eastward shift of heat accompanies an anomalous deepening of the equatorial thermocline preventing the seasonal appearance of the equatorial cold tongue. Observational programs conducted during two years in which unusually warm SSTs appeared, Equalant in 1963 (Merle 1980) and FOCAL/SEQUAL in 1984 (Carton and Hackert 1990; Reverdin et al. 1991), documented the thermocline changes during these two events.

Corresponding author address: Dr. James Carton, Department of Meteorology, University of Maryland, College Park, MD 20742-2425.

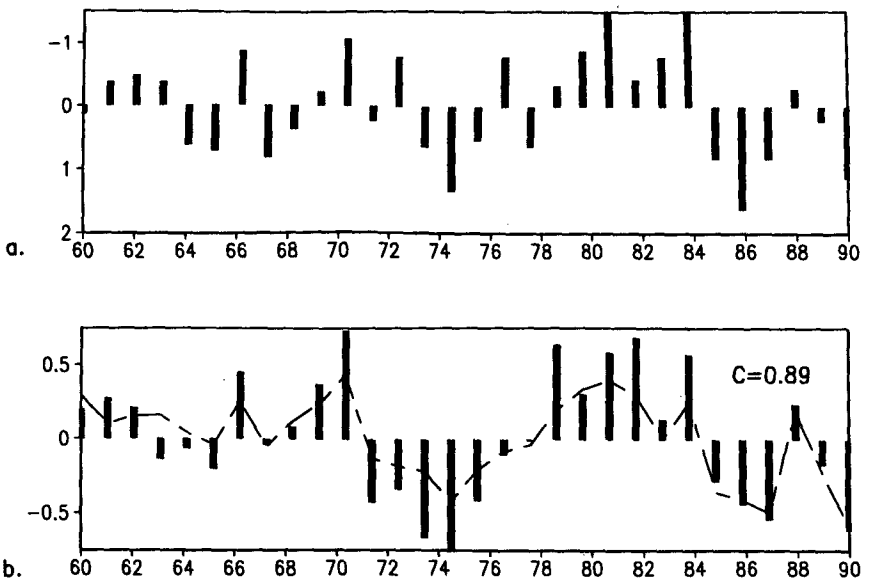

FIG. 1. (a) Normalized rainfall for the northern Nordeste region of Brazil (March–June) scaled by its standard deviations (redrawn from Hastenrath and Greischar 1993a). (b) Observed and simulated dipole indices of interhemispheric SST difference for northern spring (Mar–May) of the 30-year period 1960–1989. Observed index (histogram) has been computed from the COADS dataset. Simulated index (dashed line) has been computed from a numerical simulation of ocean dynamics forced by observed winds, also for northern spring. Index is calculated as the anomalous northern tropical SST (5°N–30°N, 60°W–10°E) minus the anomalous southern tropical SST (25°S–5°N, 60°W–10°E) in degrees (following Servain 1991). The correlation of these time series is 0.89.

Interannual anomalies of SST are superimposed on a strong seasonal cycle. Along the equator the appearance of cool water in the east is primarily associated with the intensification of the trade winds in northern summer. This cold tongue persists until the winds weaken in fall (Weingartner and Weisberg 1991). Poleward of about 10° the processes controlling the seasonal cycle of SST are distinctly different than those near the equator. At these higher latitudes the seasonal cycle of solar radiation increasingly controls the seasonal cycle of SST, rather than the winds.

Observational studies have generally not had sufficiently long records to distinguish between the factors controlling the seasonal cycle of SST and those factors controlling the interannual and longer timescales (e.g., Liu and Gautier 1990; Hayes et al. 1991). A second difficulty with these studies is evident in Hayes et al.'s conclusion that "The relatively simple correlations between SST changes and local wind on seasonal and interannual timescales are the result of a complicated interaction of variations of surface fluxes and oceanic processes." A consequence of the limited datasets available as well as the strong coupling of the atmosphere and ocean is that it is not possible to identify the dominant physical processes controlling SST from observational studies alone. It seems clear that modeling studies are required to make this separation. Recent modeling studies of the seasonal cycle and ENSO in the Pacific have generally given greater importance to surface heating processes away from the equator at interannual timescales (Seager 1989; Giese and Cayan 1993; Koberle and Philander 1994; Miller et al. 1994).

In this study we attempt to identify the major processes, both on and off the equator, that produce tropical SST anomalies on interannual to decadal timescales in the Atlantic. We begin by simulating 30 years of observed SST anomalies with a model forced by observed winds and heating during 1960–1989. We then conduct a series of experiments modifying the surface forcing fields to quantify the impact of surface heating and surface momentum flux in regulating SST.

2. Model

The ocean model used here is based on the GFDL MOM code in a domain similar to Philander and Pacanowski (1986). The horizontal resolution is 0.5° × 1.5° in the Tropics, expanding poleward of 10° to a uniform 1.5° grid at midlatitudes. The basin domain extends from 30°S to 50°N and from coast to coast for a total of 60 × 75 horizontal grid points. The vertical resolution is 15 m in the upper 150 m, expanding toward the deep ocean for a total of 20 vertical levels. Vertical mixing is Richardson number dependent, following Pacanowski and Philander (1981), while horizontal diffusion and viscosity are a constant 2×10^7

$cm^2\ s^{-1}$. The model is forced with monthly averages of daily wind stress computed from the Comprehensive Ocean Atmosphere Data Set (COADS) surface observation dataset (da Silva and Levitus 1994). Initial conditions were provided by Levitus (1982) climatological temperature and salinity.

The model is forced with the winds from 1960 for three complete years before beginning 1961 and then is run for 30 years on either a Cray YMP or a Cray C90 at Los Alamos National Laboratory. The 30-year integration requires an average of 60 hours on the Cray YMP. A second simulation is forced with climatological seasonal winds for 30 years. Simulated anomalies from the seasonal cycle (anomalies are indicated with a prime) are computed by differencing these two model runs. In this way, we minimize long-term trends due to model drift as well as eliminate the seasonal cycle.

Heat flux at the surface can be decomposed into four terms: net shortwave and longwave radiation and sensible and latent heat loss (Q = SW − LW − QE − QS). An extensive literature describes possible heat flux formulations for ocean modeling studies (see Wells and King-Hele 1990 for a review). We begin with a reasonably sophisticated parameterization of these terms. Seasonally varying SW is provided by the COADS climatological analysis of Oberhuber (1988) and is absorbed in the upper several levels of the model using a simple exponential model for light absorption. An attempt was made to examine the effects on SST of interannual variations in SW due to cloud effects. However, the inclusion of this effect led to poor simulation of observed SST and so this effect cannot be addressed in this study. Net longwave radiation is the second largest term in the surface heat flux balance, but remains approximately constant. In the east, the seasonal variation of longwave radiation is higher because of the seasonal appearance of low-level stratus clouds. We parameterize the longwave term, following Rosati and Miyakoda (1988), in terms of SST:

$$\mathrm{LW} = \epsilon\sigma \mathrm{SST}^4[0.39 - 0.5(10^{9.4-2353/\mathrm{SST}})^{1/2}] + 4\epsilon\sigma \mathrm{SST}^3. \quad (2)$$

The third largest term, latent heat loss, is a function of SST, air temperature, relative humidity, and surface wind speed. Latent heat loss is reduced over the cooler eastern waters during northern summer, as well as in low wind regions such as along the equator in northern winter. Latent heat loss is parameterized as

$$\mathrm{QE} = \rho C_p L |U_a|[\exp(\mathrm{SST}) - \gamma \exp(\mathrm{SST} - \delta T)](0.622/p_a), \quad (3)$$

where $\delta T \equiv \mathrm{SST} - T_a$. Relative humidity γ is assumed to be a constant 0.8, consistent with Philander and Pacanowski (1986). Ideally, one would like to parameterize air temperature T_a in terms of a predicted variable such as SST as has been done, for example, by Seager (1989). However, doing so leads to unacceptable systematic temperature drift during long integrations. We adopt a compromise in which δT is given by a combination of the observed and simulated SST and the monthly climatological air temperature: $(\mathrm{SST}/2 + \overline{\mathrm{SST}_{\mathrm{obs}}} - \overline{T_{a\mathrm{obs}}})/2$. Here $\overline{\mathrm{SST}_{\mathrm{obs}}}$ and $\overline{T_{a\mathrm{obs}}}$ are the annual average climatological SST and air temperatures. This formula ensures that the model does not develop unacceptable systematic drift, but at the same time we do not inappropriately specify the SST field (which we are studying!). This formula is similar to that suggested by Giese and Cayan (1993).

Sensible heat loss is given by

$$\mathrm{QS} = \rho C_D C_p |U_a|(\delta T). \quad (4)$$

It is through these last two terms (mainly QE) that air temperature provides a negative feedback on simulated SST (although the applicability of this feedback mechanism has been questioned by Liu and Gautier 1990). When all terms are included, the net heat flux at the surface of the model varies seasonally between ±50 $W\ m^{-2}$, similar to estimates of modern climatologies.

In addition to the basic simulation, four additional experiments will be presented. The first two experiments will examine the importance of equatorial wind anomalies in generating equatorial SST anomalies. The third and fourth experiments examine the relative importance of ocean dynamics and surface heat flux in generating primarily off-equatorial SST anomalies.

3. Gross statistics

In this section we examine processes controlling anomalies of SST (SST′) from their climatological seasonal cycle. We begin by comparing the spatial distribution of possible forcing functions to the spatial distribution of SST′. One potential mechanism for regulating SST′ is the variation of vertical flux of cool water into the mixed layer due to variations in Ekman pumping and thus to anomalies of wind stress. Anomalies of the wind stress curl increase in amplitude in the subtropics where the wind field is regulated by oceanic high pressure systems (Fig. 2a). A second potential mechanism is the variation in net surface heat flux. The amplitude of heat flux anomalies also increases in the subtropics, partly because of the increase in SST variability and partly because of the increase in anomalous winds, which also enter the calculation of surface heating (Fig. 2b).

Variability of observed SST′ (Fig. 3a) increases somewhat near the equator. It is typically about 0.5°C, with somewhat lower values in the west and higher values south of 15°S and near the eastern boundary. This distribution of SST′ is strikingly different from the Pacific where the SST′ signal near the equator overwhelms signals elsewhere. Simulated SST′ in the Atlantic (Fig. 3b) has a similar pattern although reduced in amplitude by 20%. We believe that this re-

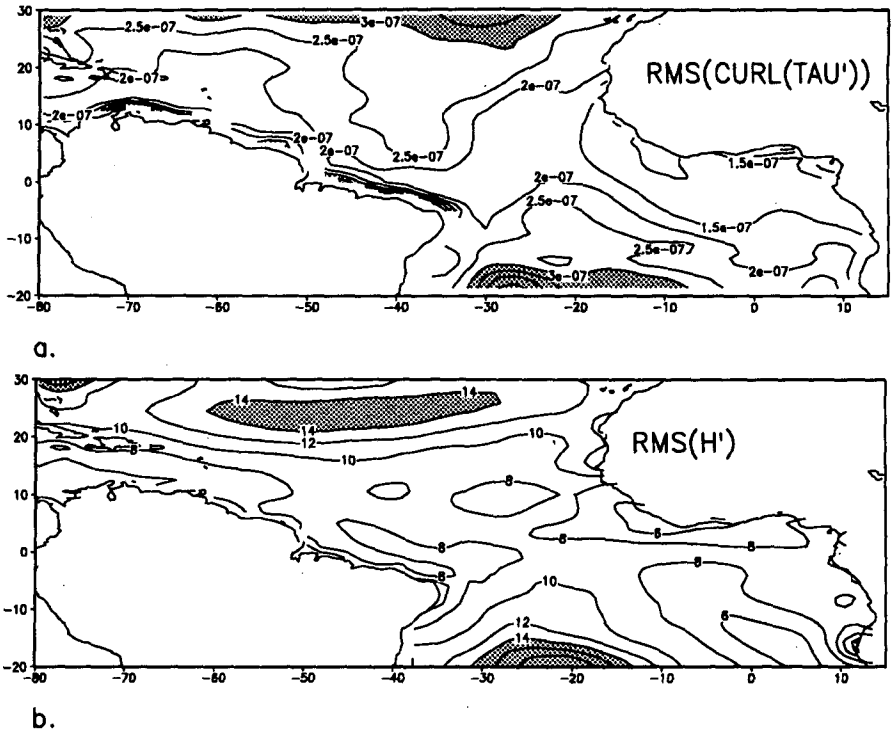

FIG. 2. (a) Root-mean-square of the anomalous wind stress curl computed from the 30-year record. Contour interval is 0.5×10^{-7} dyn cm^{-2} m^{-1}. Regions exceeding $3. \times 10^{-7}$ dyn cm^{-2} m^{-1} are shaded. (b) Root-mean-square of the anomalous net surface heat flux computed from the model simulation. Contour interval is 2 W m^{-2}. Regions exceeding 14 W m^{-2} are shaded.

duction in amplitude of the anomalies is due to the approximation of δT required to minimize climate drift.

Heat storage in the tropical oceans occurs mainly through vertical movements of the thermocline (Katz 1987), which is represented here by the depth of the 20°C isotherm. Seasonally, the thermocline undergoes fluctuations of between 10 and 20 m. The simulated anomalies are generally smaller than this, in the range 3–8 m (Fig. 3c). As in the case of SST′, there is a weak increase in variability of thermocline depth near the equator.

The correlation between anomalies of SST and thermocline depth provide an interesting contrast to the Pacific. In the equatorial Pacific anomalies of SST result from zonal shifts of excess oceanic heat content (Zebiak 1989). Fluctuations in the depth of the thermocline are strongly correlated with anomalies of SST and both are amplified near the equator. In the tropical Atlantic, in addition to weaker amplification, areas of strongly positive correlation between anomalous thermocline depth and anomalous SST are limited to the eastern equatorial zone (Fig. 3d). This result already suggests that if ENSO-type air–sea interactions exist in the tropical Atlantic, as suggested by Zebiak (1993) and Carton and Huang (1994), then they are confined to this region.

4. Variability on the equator

In this section we examine time series of anomalies for the eastern region where anomalous thermocline depth and anomalous SST are well correlated (6°S–2°N, 20°W–10°E). It is evident from the observed SST′ record (Fig. 4a) that a series of nine warm events have occurred in the three decades beginning in 1960 (1963, 1966, 1968, 1973, 1974, 1981, 1984, 1987, and 1988; here we define a warm event as one exceeding 0.5°C for at least three months). Five cool events have also occurred during this period (1964, 1967, 1969, 1976, and 1978). The warm events are primarily confined to the months June through August (tick marks have been placed in Fig. 4 to mark July of years with warm events, while the cool events occur irregularly throughout the year). Comparison with the zonal wind stress anomalies in Fig. 4d shows that the warm events are generally preceded by a relaxation of the trade winds (an increase in the trade wind anomaly) in either winter or spring preceding the warming.

The simulated SST′ in the eastern Atlantic (superimposed on the observed SST′ in Fig. 4a) reproduces warm events in 1963, 1966, 1968, and 1984. The most dramatic relaxations of equatorial trade winds occur in three years: 1963, 1968, and 1983/84. During each of

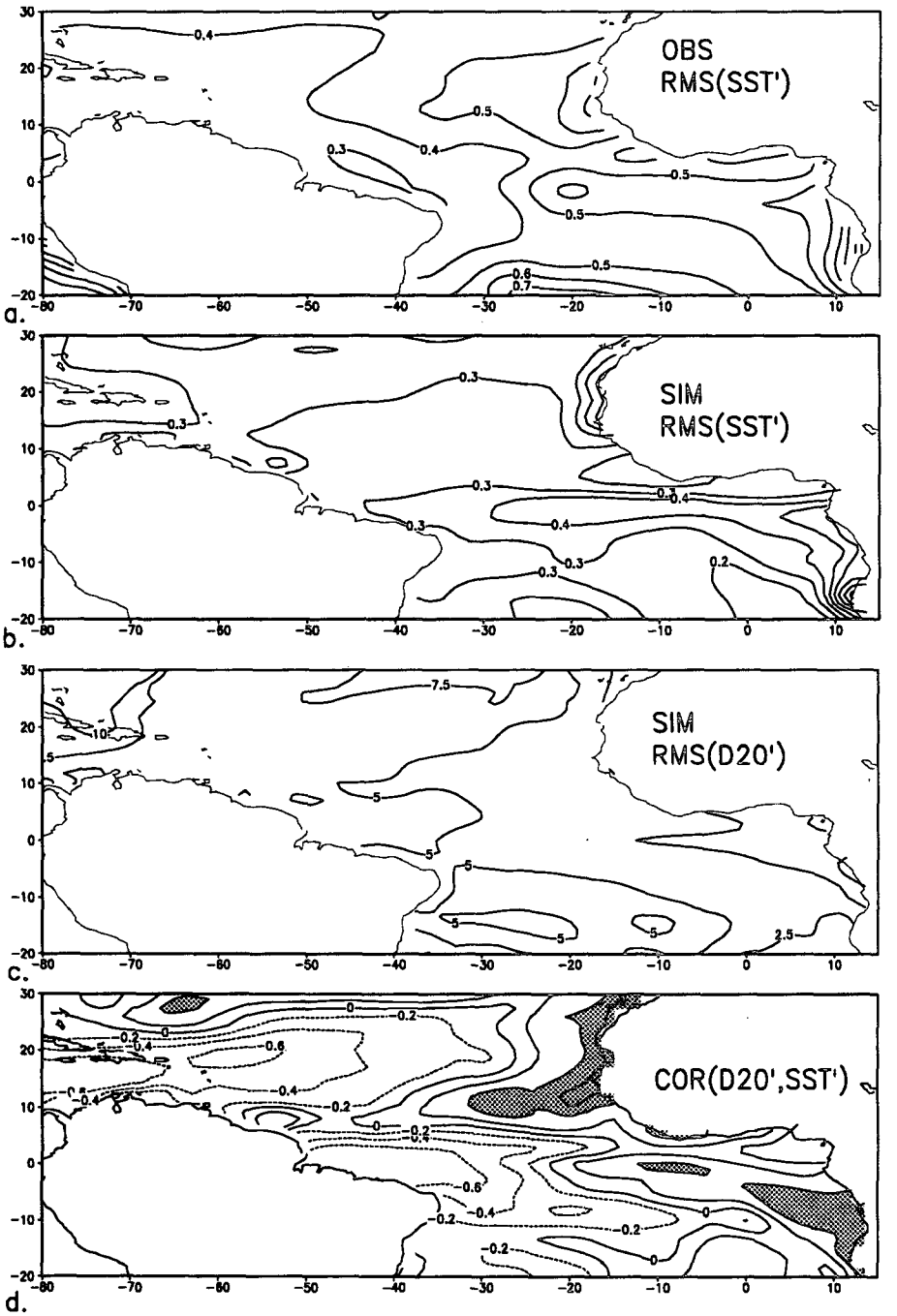

FIG. 3. Gross statistics of simulation anomalies computed from the 30-year record: (a) Root-mean-square observed SST′, (b) root-mean-square simulated SST′, (c) root-mean-square variation of the depth of the 20°C isotherm, and (d) correlation of simulated anomalies of the depth of the 20°C isotherm and simulated SST′. Correlations exceeding 0.4 are shaded. Contour intervals are 0.1°C, 2.5 m, 0.1°C and 0.2 m.

these years the winds relaxed by 0.1–0.2 dyn cm^{-2} for several months. Accompanying each wind relaxation was an anomalous deepening of the eastern thermocline by 8–15 m preceding the rise in anomalous SST. Of the observed cool events only those of 1976 and 1983/84 were well simulated. Both of these cool events were accompanied by an anomalous shallowing of the eastern thermocline (Fig. 4b). The wind anomalies in the

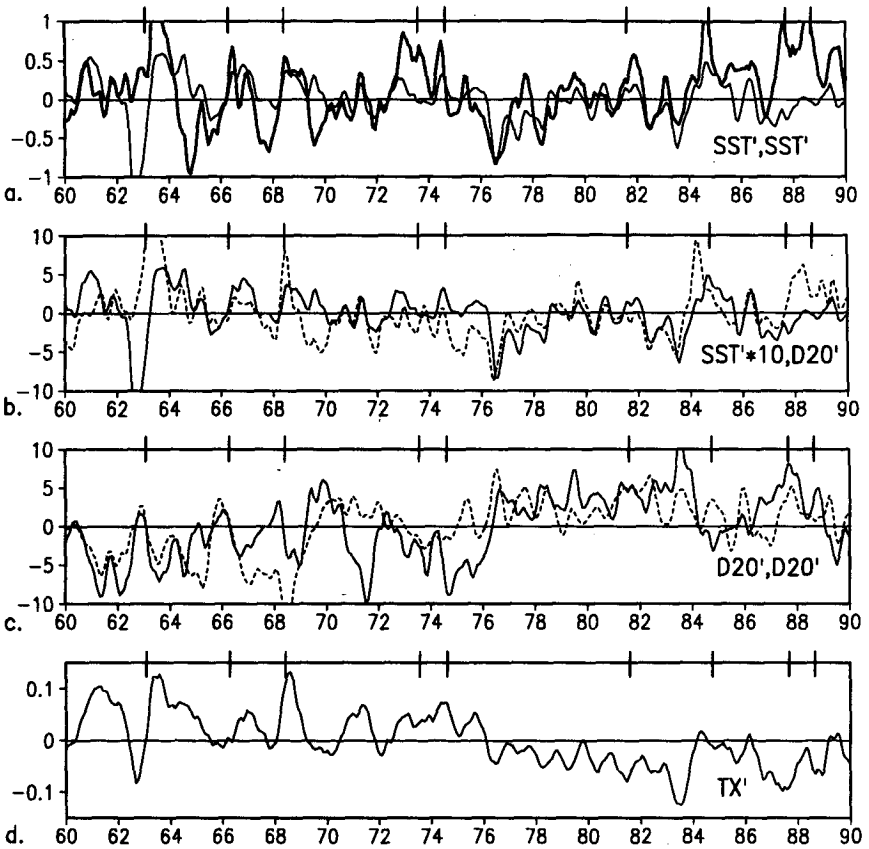

FIG. 4. Time series of anomalies from simulation, smoothed with a three-month running filter. (a) Observed (bold) and simulated (solid) SST′ in the eastern equatorial Atlantic (6°S–2°N, 15°W–10°E). Anomalous cooling in 1962 is the result of errors in the wind field. (b) Simulated (solid) SST′ and simulated D20′ (dashed) in the eastern equatorial Atlantic as defined above. (c) Simulated D20′ in the northwest (solid, 0°–10°N, 50°–35°W) and southwest (dashed, 15°–5°S, 35°–20°W). (d) Observed $\tau^{x\prime}$ along equator (2°S–2°N, 35°–25°W). Units are degrees, meters and dynes per square centimeter. Tick marks are used to indicated July of the years with warm events: 1963, 1966, 1968, 1973, 1974, 1981, 1984, 1987, and 1988.

eastern Atlantic are weaker by a factor of 3 than the wind anomalies in the eastern Pacific. Thus, it is not surprising that the simulated SST and heat content anomalies are poorly simulated (correlations of 0.33 and 0.34).

A previous examination of the heat budget of the tropical Atlantic by Carton and Huang (1994) shows that the majority of the anomalous heat transported into the eastern equatorial ocean came from the western tropical ocean. Figure 4c shows time series of the anomalous thermocline depth variations in two regions north and south of the equator. Comparison with the thermocline depth variations in the eastern region shows that in different years differing amounts of heat are stored north or south of the equator. We can conclude, for example, that in 1966 the southern region was most responsible for supplying heat to the east because the simulated thermocline rose 10 m in the south while it rose only 5 m in the north. The situation was reversed in 1984 when the major export of heat occurred north of the equator where the simulated thermocline rose 13 m.

Success in invoking the ENSO mechanism to explain these fluctuations of SST requires that they be primarily related to equatorial wind variations. However, the narrow width of the tropical Atlantic basin suggests that off-equatorial winds may be important as well. Here we estimate how much of the SST′ signal can be explained by off-equatorial winds. In both experiments, which we call experiments 1 and 2, the simulation is repeated with a modified wind field. In experiment 1 the winds near the equator are replaced by climatological seasonal winds, while the complete wind field is specified poleward of 5°. To eliminate a sudden transition between climatological and complete winds, the transition between the two is specified as

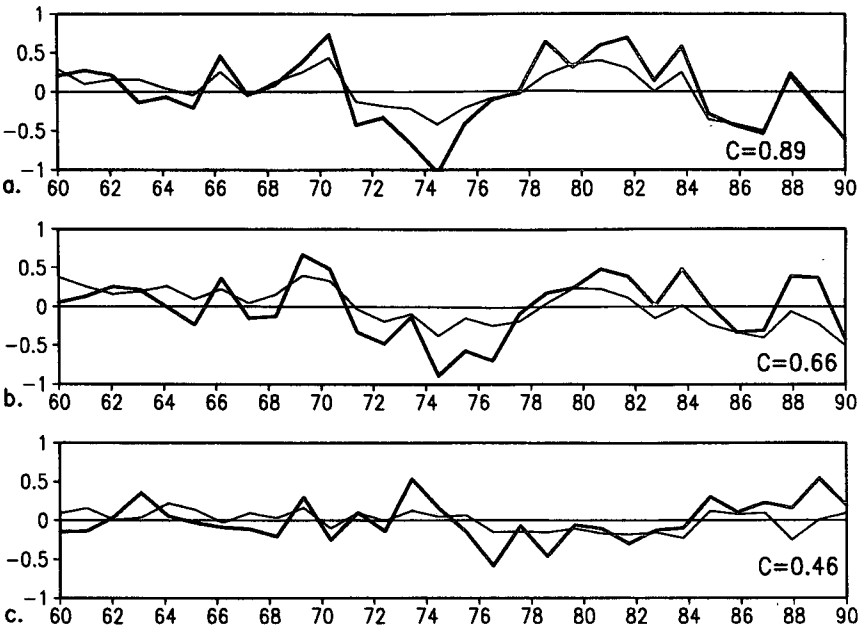

FIG. 5. Dipole index of SST anomaly computed over the months of March–May. Observed (solid) and simulated (dashed). (a) Interhemispheric differences similar to those shown in Fig. 1. (b) Northern Hemisphere anomalies (define following Servain 1991 as 5°–30°N, 60°W–15°E). (c) Southern Hemisphere anomalies (25°S–5°N, 60°W–15°E). Correlations are shown in the lower right-hand corner.

$$\vec{\tau} = \vec{\tau}_{\text{cli}}, \quad |\theta| < \lambda$$

$$\vec{\tau} = \begin{cases} \vec{\tau}_{\text{cli}}\left[\cos\left(\pi\dfrac{\theta-\lambda}{5^\circ}\right)+\dfrac{1}{2}\right] \\ \quad + \vec{\tau}_{\text{obs}}\left[\dfrac{1}{2}-\cos\left(\pi\dfrac{\theta-\lambda}{5^\circ}\right)\right], \\ \qquad\qquad\qquad\qquad \lambda < |\theta| < \lambda + 5^\circ \\ \vec{\tau}_{\text{obs}}, \quad |\theta| < \lambda + 5^\circ, \end{cases}$$

where $\lambda = 0$. The root-mean-square (rms) of the average SST′ (6°S–2°N, 20°W–10°E) is reduced by 45% from 0.31° to 0.17°C. In experiment 2 λ is expanded to 2.5° so that climatological winds extend to 7.5° off the equator. The rms SST in the eastern equatorial Atlantic is further reduced to 0.09°C. These experiments show that *wind anomalies displaced from the equator by more than 7.5° contribute little to the eastern equatorial SST anomalies.*

5. Interhemispheric variability

As is apparent from Fig. 1, the interhemispheric difference in SST′ strongly influences the position of convective zones and thus the low-level circulation throughout the Tropics. The zonally averaged anomalies are typically 0.5°C in the Northern Hemisphere with weaker 0.25°C anomalies in the Southern Hemisphere. Off-equatorial anomalies appear to have longer decadal timescales than near the equator. Also superimposed on the lower panel of Fig. 1 is the simulated interhemispheric difference of SST′. The correlation between the simulation and observations is high.

We examine the agreement between observed and simulated SST′ in Fig. 5. In the Northern Hemisphere, where the largest anomalies occur, the observed and simulated time series have a correlation of 0.66. The interhemispheric difference of SST′ has a better agreement with observations than the comparisons for a single hemisphere (correlation of 0.89) reflecting the larger amplitude of the signal. The uncertainty in the correlation estimates is large due to the presence of energy on 5 to 10 year timescales. A clue to the possible causes of the interhemispheric differences of SST′ is shown in Fig. 6a. The interhemispheric difference of zonal wind stress reveals a close correspondence to the interhemispheric difference of SST′ (reproduced from Fig. 5a in Fig. 6c). Likewise, years with a southward gradient of SST′, such as occurred in the early 1970s, are also years with a northward gradient of anomalous tradewinds. For example, in 1974 SSTs were anomalously warm in the Southern Hemisphere. This was a period in which the trade winds were anomalously weak in the Southern Hemisphere. Years with a northward gradient of SST′ are years with a southward gra-

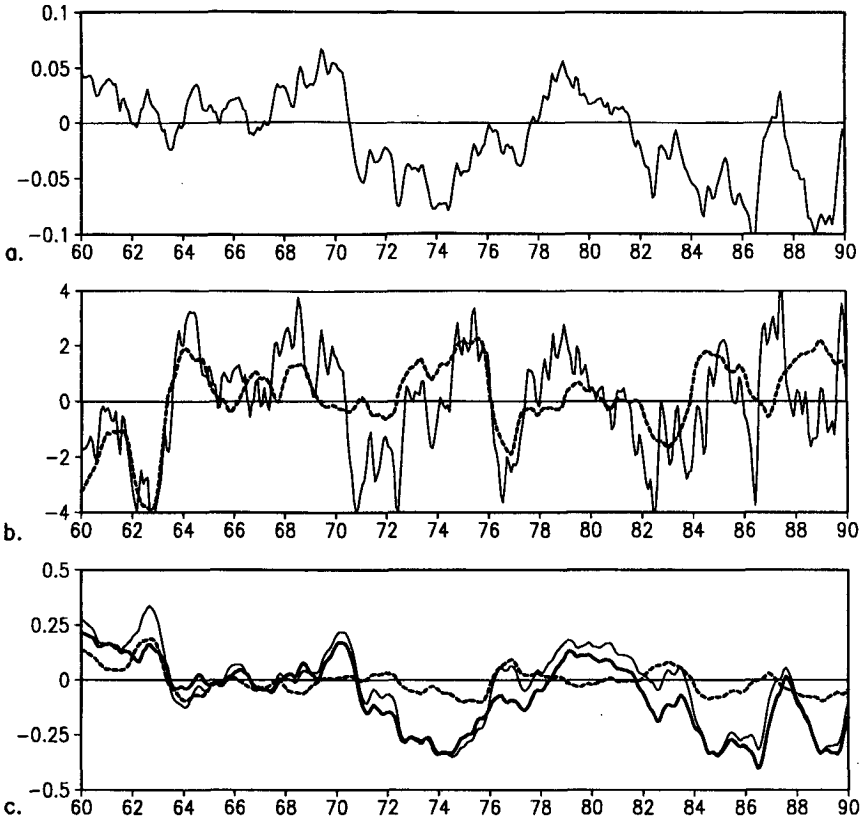

FIG. 6. Time series of 12-month smoothed interhemispheric differences of variables from the simulation. (a) Surface wind stress anomaly. (b) heat content anomaly, and (c) SST anomaly. Results from the simulation are shown with a solid line. Results from experiment 3 and experiment 4 are also displayed. In experiment 3 the effect of interannual variations in latent cooling due to interannual fluctuations in wind speed are eliminated (short dashed line). In experiment 4 interannual variations in latent cooling are retained, but the contribution of the interannual variations in the winds in driving anomalous ocean circulation is eliminated (long dashed line). For all other calculations climatological winds are used.

dient of anomalous trade winds. In order to separate the causes of SST′ variation from the effects of that variation on winds and heating, we conduct experiments 3 and 4.

To determine the importance of wind stress anomalies in dynamically forcing changes in SST, the surface heat flux is modified in experiment 3 by replacing wind speed in the calculation of latent heating [Eq. (3)] with its climatological seasonal values. In experiment 4 the full latent heating is retained; however, wind stress in the momentum equations is replaced with its climatological seasonal mean values. The results are summarized in Figs. 6b,c.

The result of using monthly climatological wind speed in the bulk formula for latent heat loss is dramatic. By eliminating the anomalous wind-evaporation most of the interannual variability of SST disappears (Fig. 6c), even though the change to surface heat flux is less than 4 W m^{-2} (Fig. 6b). The reduction in SST′ variability occurs poleward of ±5° (Fig. 7a). Closer to the equator SST′ is primarily controlled by wind stress and so SST′ variability remains large. Since thermocline variations are primarily controlled by dynamical effects, the thermocline variability remains unaffected (Fig. 7b).

In experiment 4 the anomalous wind evaporation is retained, but the effect of wind stress in driving anomalous currents and thermocline variations is eliminated. The SST′ gradient in this experiment virtually reproduces the control case with a 0.95 correlation and explains 89% of the variance of the control case (Fig. 6c). At the same time SST′ variability is reduced within ±5° of the equator and thermocline variability is reduced throughout much of the tropical ocean.

One exception to this conclusion occurs in the coastal regions of the eastern Atlantic. In this region, SST′ variability depends on other processes such as alongshore fluctuations in wind stress, not on fluctuations in surface heating (compare Fig. 7a,c with Fig. 3b). Thus, we conclude that coastal upwelling controls

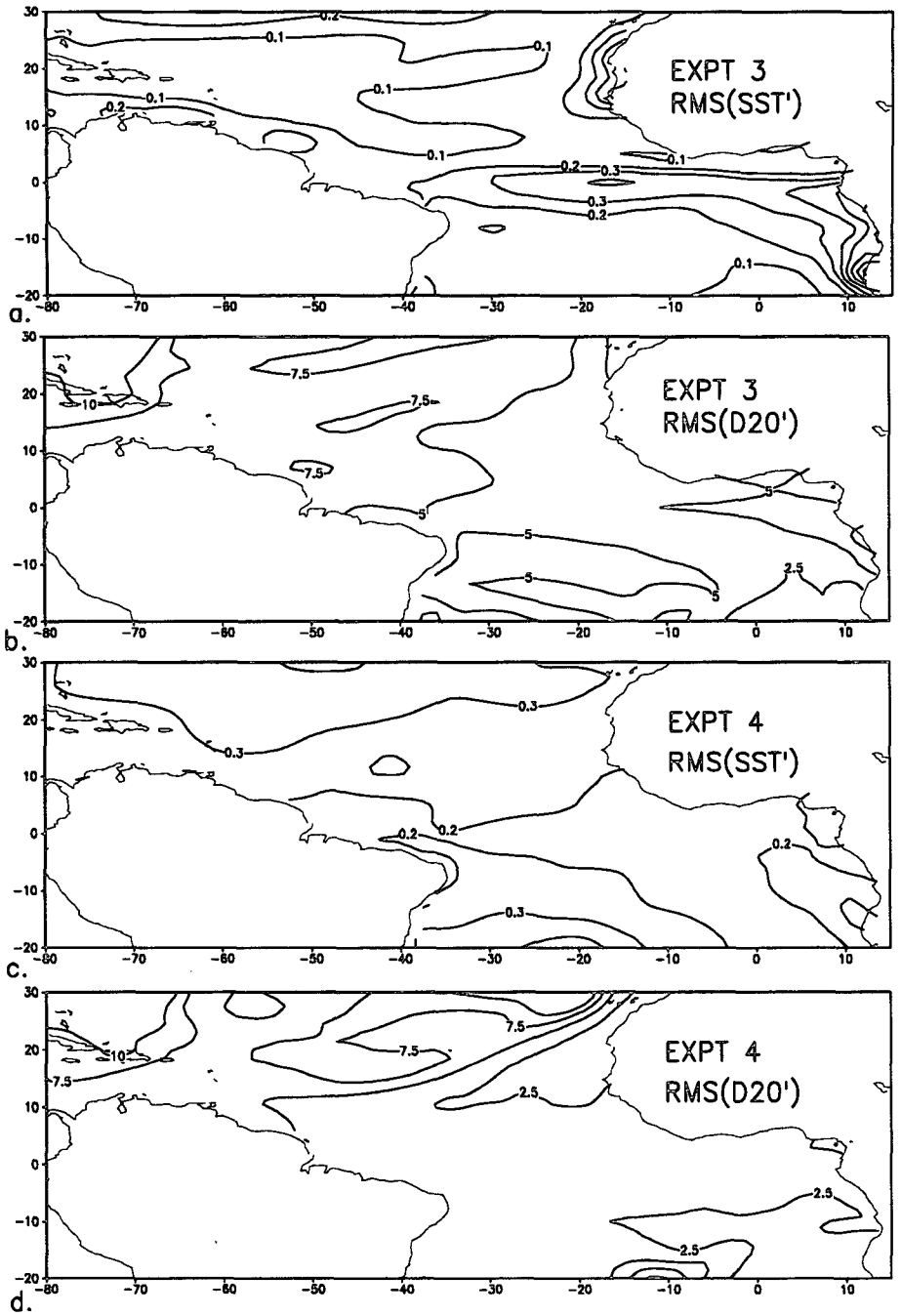

FIG. 7. Gross statistics for the third and fourth interannual variability experiments. The third interannual variability experiment has the wind effect in the calculation of latent heating replaced by its climatological seasonal cycle. The fourth interannual variability experiment has climatological seasonal wind stress. Left-hand panels show root-mean-square SST′. Right-hand panels show root-mean-square of the anomalous depth of the 20°C isotherm.

SST′ close to the coast of northwest Africa. More than a few hundred kilometers from the coast surface fluxes are more important than thermocline variations or horizontal advection in controlling SST′.

6. Conclusions

This is a study of the causes of the anomalies of SST in the tropical Atlantic, particularly those anomalies re-

lated to climate. SST anomalies in the tropical Atlantic have weak variability compared to the Pacific and are more broadly distributed geographically. Surprisingly, despite the weaker nature of the SST anomalies, features of their interannual and decadal variability may be reproduced with significant accuracy using climatological wind products. In contrast to the Pacific where there has been considerable success in reproducing SST anomalies associated with ENSO, it is striking that the off-equatorial SST anomalies in the Atlantic are better reproduced than the equatorial SST anomalies. The explanation for the difference in the success of the simulation of SST anomalies lies in the differing causes of SST fluctuations in the two regions.

Near the equator the strongest variations of SST occur in the eastern ocean. Anomalously warm SSTs are generally associated with an anomalous deepening of the thermocline in this region during the Northern Hemisphere summer. The excess warm water is supplied from either the northwestern or the southwestern basin in response to a relaxation of the trade winds. By comparing simulations with and without anomalous wind variability, we are able to demonstrate that most of the SST variability results from wind anomalies within $\pm 7.5°$ of the equator. This result has implications for the construction of an observing system. Such a small area could easily be instrumented with a limited number of ATLAS-type moorings. The simulation reported here shows that the major sources of the excess heat may be either the northwestern or the southwestern tropical ocean. Thus, monitoring the storage of excess heat will require measurements in both hemispheres.

Anomalies of SST away from the equator are nearly as large as the equatorial anomalies and also have important climate effects. One striking example of the climate impact of off-equatorial SST anomalies is the relationship between interhemispheric differences of SST and rainfall anomalies in the northern Nordeste region of Brazil (Fig. 1). Warm southern SSTs relative to northern SSTs cause a southward shift of the atmospheric intertropical convergence zone and thus an increase in rainfall.

A number of processes could potentially give rise to SST variations including changes in cloudiness, evaporation, local wind-driven effects, remote effects due to changes in coastal upwelling, and changes in inter- and intrahemispheric heat transports. In this study we are able to distinguish among most of these factors with the exception of cloudiness. Of the factors that we are able to examine, we find that the effect of varying winds in latent heat loss from the surface is by far the most important mechanism. When this effect is included, the observed SST anomaly record can be simulated with considerable accuracy (as illustrated in Fig. 1, lower panel). Without this effect, the anomalies are weak and correlate poorly with the observations.

These experiments provide convincing evidence that the interhemispheric patterns of anomalous SST result from low-frequency changes in evaporation and are relatively decoupled from thermocline variations. This mechanism will be most effective at low frequencies because of the integrating effect of the heat balance in the mixed layer. Thus, the interhemispheric pattern of SST variation has energy at long decadal timescales, even though the winds vary on both shorter and longer timescales. This result is consistent with the high correlation between these variables and SST tendency, as pointed out by Cayan (1992). The anomalies of heat flux associated with the interhemispheric gradient of SST′ are well below the observational limit of 10–20 W m^{-2} typically assumed for heat flux calculations. This means that it will not be possible to verify the role of surface fluxes by direct observation.

Acknowledgments. This work was supported by the National Oceanic and Atmospheric Administration NA56GP0472 and the National Science Foundation OCE9416894. We are grateful to S. Hastenrath and L. Greischar for providing the rainfall time series.

REFERENCES

Carton, J. A., and E. Hackert, 1990: Data assimilation applied to the temperature and circulation in the tropical Atlantic, 1983–84. *J. Phys. Oceanogr.*, **20,** 1150–1165.

——, and B. Huang, 1994: Warm events in the tropical Atlantic. *J. Phys. Oceanogr.*, **24,** 888–893.

Cayan, D. R., 1992: Latent and sensible heat flux anomalies over the northern oceans: Driving the sea surface temperature. *J. Phys. Oceanogr.*, **22,** 859–881.

da Silva, A. M., and S. Levitus, 1994: *Atlas of Surface Marine Data 1994.* Vol. 1, *Algorithms and Procedures.* National Oceanic and Atmospheric Administration, 83 pp.

Folland, C. K., T. N. Palmer, and D. E. Parker, 1986: Sahel rainfall and worldwide sea temperatures. *Nature,* **320,** 602–606.

Giese, B. S., and D. R. Cayan, 1993: Surface heat flux parameterizations in tropical sea surface temperature simulations. *J. Geophys. Res.,* **98,** 6979–6989.

Gray, W., and J. D. Sheaffer, 1991: *Teleconnections Linking Worldwide Climate Anomalies.* M. H. Glantz, R. W. Katz, and N. Nicholls, Eds., Cambridge University Press, 535 pp.

Hastenrath, S., and L. Greischar, 1993a: Further work on the prediction of Brazilian rainfall anomalies. *J. Climate,* **6,** 734–758.

——, and ——, 1993b: Circulation mechanisms related to Northeast Brazil rainfall anomalies. *J. Geophys. Res.,* **98,** 5093–5102.

Hayes, S. P., P. Chang, and M. J. McPhaden, 1991: Variability of the sea surface temperature in the eastern equatorial Pacific Ocean. *J. Geophys. Res.,* **96,** 10 553–10 566.

Hisard, P., 1980: Observation de response du type "El Niño" dans l'Atlantique tropical oriental—Golfe de Guinee. *Ocean. Acta,* **3,** 69–78.

Katz, E. J., 1987: Seasonal response of the sea surface to the wind in the equatorial Atlantic. *J. Geophys. Res.,* **92,** 1885–1893.

Koberle, C., and S. G. H. Philander, 1994: On the processes that control seasonal variations of sea surface temperatures in the tropical Pacific Ocean. *Tellus,* **46,** 481.

Lamb, P. J., and R. A. Peppler, 1991: West Africa. *Teleconnections Linking Worldwide Climate Anomalies,* M. Glantz, R. W. Kexitatz, and N. Nicholls, Eds., Cambridge University Press, 121–189.

Levitus, S., 1982: *Climatological Atlas of the World Ocean.* NOAA Prof. Paper No. 13, U.S. Govt. Printing Office, 173 pp. and 17 microfiche.

Liu, W. T., and C. Gautier, 1990: Thermal forcing on the tropical Pacific from satellite data. *J. Geophys. Res.,* **95,** 13 209–13 217.

Merle, J., 1980: Variabilite thermique et interannuelle de l'Ocean Atlantique equatorial Est. L'hypothese d'un "El Niño" Atlantique. *Ocean. Acta,* **3,** 209–220.

Miller, A. J., D. R. Cayan, T. P. Barnett, N. E. Graham, and J. M. Oberhuber, 1994: Interdecadal variability of the Pacific Ocean: Model response to observed heat flux and wind stress anomalies. *Climate Dyn.,* **9,** 287–302.

Oberhuber, J. M., 1988: *An Atlas based on the "COADS" Data Set: The Budgets of Heat, Buoyancy and Turbulent Kinetic Energy at the Surface of the Global Ocean.* Max-Planck Institute for Meteorology/Hamburg, Report No. 15.

Pacanowski, R. C., and S. G. H. Philander, 1981: Parameterization of vertical mixing in numerical models of tropical oceans. *J. Phys. Oceanogr.,* **11,** 1443–1451.

Philander, S. G. H., and R. C. Pacanowski, 1986: A model of the seasonal cycle of the tropical Atlantic Ocean. *J. Geophys. Res.,* **91,** 14 192–14 206.

Reverdin, G., P. Delecluse, C. Levy, P. Andrich, A. Moliere, and J. M. Verstraete, 1991: The nearsurface tropical Atlantic in 1982–4: Results from a numerical simulation and a data analysis. *Progress in Oceanography,* Vol. 27, Pergamon, 273–340.

Rosati, A., and K. Miyakoda, 1988: A general circulation model for upper ocean circulation. *J. Phys. Oceanogr.,* **18,** 1601–1626.

Seager, R., 1989: Modeling tropical Pacific sea surface temperature: 1970–87. *J. Phys. Oceanogr.,* **19,** 419–434.

Servain, J., 1991: Simple climate indices for the tropical Atlantic Ocean and some applications. *J. Geophys. Res.,* **96,** 15 137–15 146.

Wagner, R. G., and A. da Silva, 1994: Surface conditions associated with anomalous rainfall in the Guinea coastal region. *Int. J. Climatol.,* **14,** 179–199.

Weingartner, T. J., and R. H. Weisberg, 1991: A description of the annual cycle in sea surface temperature and upper ocean heat in the equatorial Atlantic. *J. Phys. Oceanogr.,* **21,** 83–96.

Wells, N. C., and S. King-Hele, 1990: Parameterization of tropical ocean heat flux. *Quart. J. Roy. Meteor. Soc.,* **116,** 1213–1224.

Zebiak, S. E., 1989: Oceanic heat content variability and El Niño cycles. *J. Phys. Oceanogr.,* **19,** 475–486.

——, 1993: Air–sea interaction in the equatorial Atlantic region. *J. Climate,* **6,** 1567–1586.